Understanding the Spatiotemporal Structures in Atmosphere-Land Surface Exchange at the Jülich Observatory for Cloud Evolution

Marke[1], T., S. Crewell[1], U. Löhnert[1], U. Rascher[2]

[1] *Institute of Geophysics and Meteorology, University of Cologne,* [2] *Research Center Jülich, IBG-2*

1. JOYCE-CF Ground Based Observations and Site Characteristics

Fig. 1: *JOYCE-CF Instruments (left to right): Doppler lidar, Microwave Radiometer, Ceilometer, Cloud Radar, 120 m Meteorological Tower and Eddy Covariance station.*

The Jülich Observatory for Cloud Evolution Core Facility (**JOYCE-CF**) provides a diverse set of instruments (Fig. 1) for continuous and highly-resolved measurements of the **boundary layer** since 2011. Together with a heterogeneous environment in terms of topography and land use, the **interactions** between atmosphere and land-surface can be observed.

Fig. 2: *Map showing the location of the JOYCE site (red marker) and the estimated area (5 km radius) influencing the MWR scans (green circle).*

2. Plant Induced Water Vapor Variability in the Atmosphere

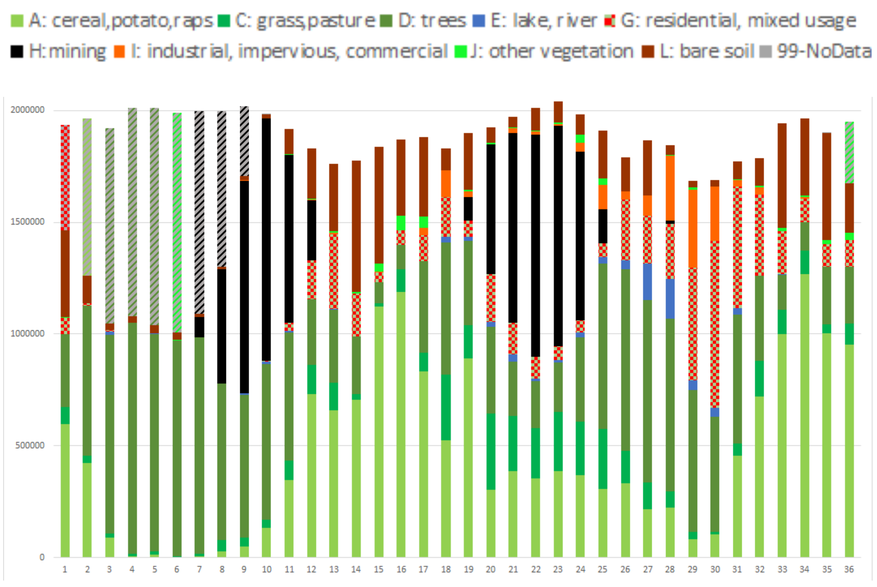

Fig. 3: *Distribution of active vegetation and other land use classes [3] for a 5 km radius (Fig. 2) around JOYCE in 10° azimuth steps.*

- **Land use**: large variability around the JOYCE-CF site (Fig. 3)
- **Assumption**: heterogeneity causes spatial differences in the water vapor field
- **First case analysis**: the water band index (WBI) derived from the high-performance airborne imaging spectrometer HyPlant [2] shows directional variations that can also be seen in the integrated water vapor (IWV) measurements by a microwave radiometer (MWR) and the MODIS Terra/Aqua satellites (Fig. 4)
- **Future work**: select suitable days using a boundary layer classification (see 3) to investigate the correlation between IWV distribution and plant phenology

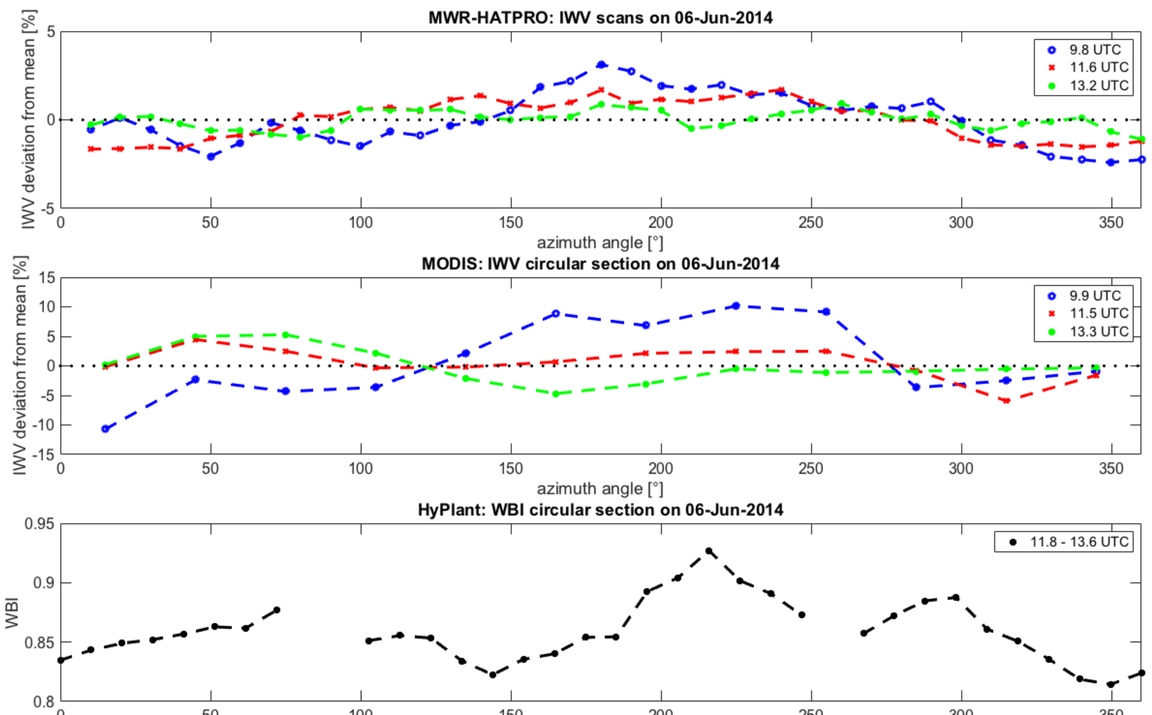

Fig. 4: *Deviation from the mean IWV depending on the azimuth angle derived from MWR scans (top) and from a MODIS circular section (center). The bottom panel shows the WBI derived from a circular section of the HyPlant flights on 06-Jun-2014.*

3. Boundary Layer Classification Based on Doppler Lidar

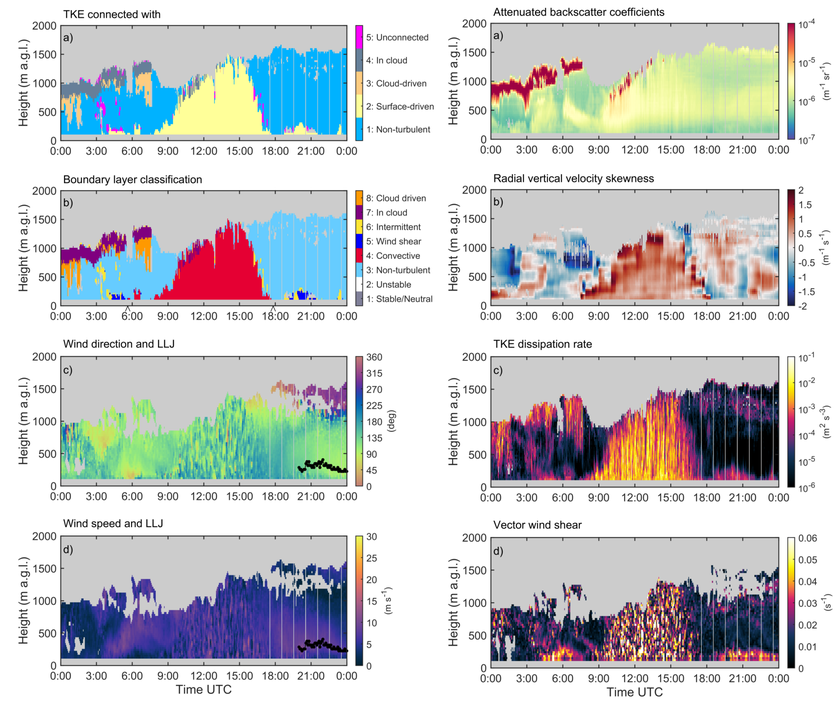

Fig. 5:
Left: Time-height plots of boundary layer classification showing a) connection with the surface (i.e. surface-driven versus cloud-driven), and b) the turbulent mixing source, together with c) wind direction, and d) wind speed on 24 March 2018 at JOYCE-CF.

Right: Time-height plots of of a) attenuated backscatter coefficient, b) vertical velocity skewness, c) TKE dissipation rate, and d) vector wind shear, calculated from Doppler lidar measurements on 24 March 2018 at JOYCE-CF.

- **Concept:** Single instrument data product [4] for operational classification of the evolution of mixing processes and detecting the origin of turbulence.
- **Applications:**
  - Identify specific situations for long-term analysis of land surface-atmosphere coupling
  - Evaluation of Large-Eddy-Simulations (LES)
  - Large potential for Doppler lidar network

4. Clear Sky Convective Boundary Layer Statistics

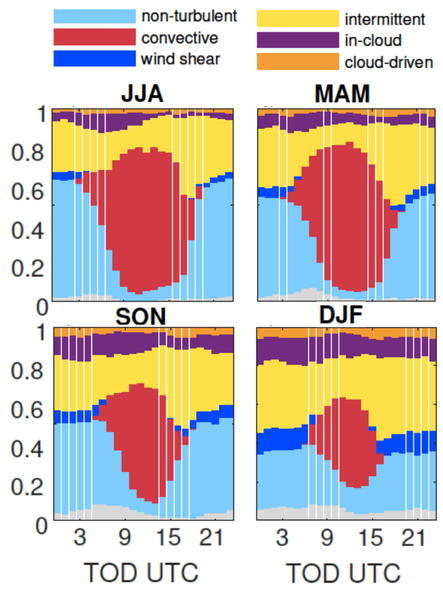

Fig. 6: *Seasonal average diurnal cycle of the probability for each identified boundary layer class over JOYCE-CF between 105-555 m from May 2015 – December 2016.*

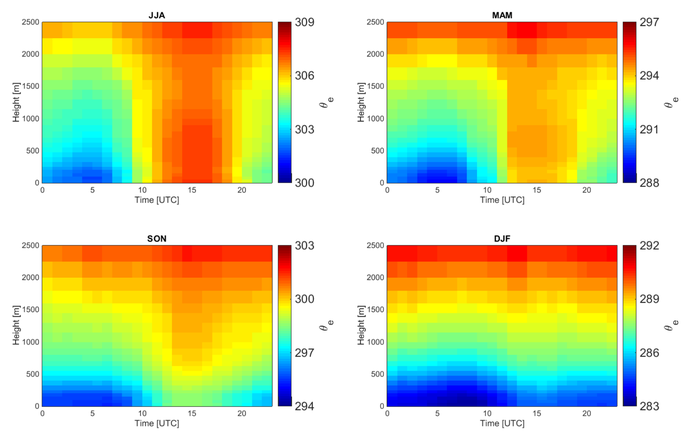

Fig. 7: *Seasonal mean diurnal cycle of equivalent potential temperature for clear sky cases between 2012-2018.*

The **long-term** application of the boundary layer classification (Fig. 6) allows for an evaluation of e.g. clear sky **convective** cases, showing clear seasonal and diurnal variations in the equivalent potential temperature (Fig. 7), water vapor variability (Fig. 8) and a **connection** to the height of the boundary layer (Fig. 9).

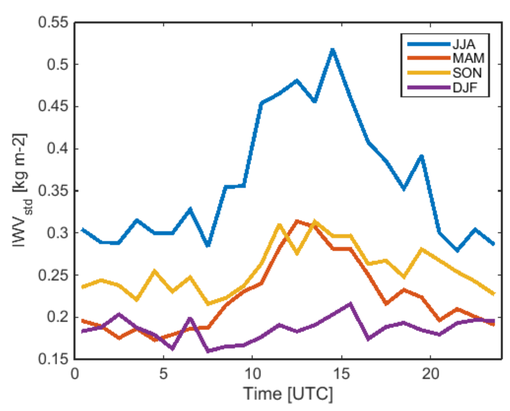

Fig. 8: *Hourly mean values of the clear sky IWV standard deviation divided into seasons between 2012-2018.*

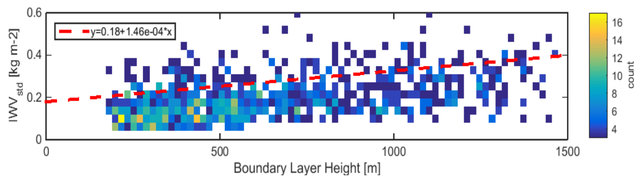

Fig. 9: *Hourly mean values of boundary layer height vs IWV standard deviation (red dashed line: linear fit) for clear sky convective cases.*

References:

[1] J. Schween, S. Crewell, U. Löhnert: Horizontal humidity gradient from one single scanning microwave radiometer, IEEE Trans. Geosci. Remote Sens., vol. 8, no. 2, pp. 336-340, 2010.

[2] U. Rascher et al.: Sun-induced fluorescence - a new probe of photosynthesis: First maps from the imaging spectrometer HyPlant, Global change biology, vol. 21, 2015.

[3] G. Waldhoff, U. Lussem, G. Bareth: Multi-Data Approach for remote sensing-based regional crop rotation mapping: A case study for the Rur catchment, Germany, International Journal of Applied Earth Observation and Geoinformation, vol. 61, pp 55-69, 2017.

[4] A. J. Manninen, T. Marke, M. Tuononen, E. J. O'Connor: Atmospheric boundary layer classification with Doppler lidar, submitted to JGR Atmospheres, 2018.

tmarke@meteo.uni-koeln.de